Sleep homeostasis reflects temporally integrated local cortical neuronal activity

Christopher W. Thomas[1], Mathilde C. C. Guillaumin[2], Laura E. McKillop[1], Peter Achermann[3,4], Vladyslav V. Vyazovskiy[1]*

[1] Department of Physiology, Anatomy and Genetics, University of Oxford, Oxford, UK; [2] Nuffield Department of Clinical Neurosciences, University of Oxford, Oxford, UK; [3] Institute of Pharmacology and Toxicology, University of Zurich, Zurich, Switzerland; [4] The KEY Institute for Brain-Mind Research, Department of Psychiatry, Psychotherapy and Psychosomatics, University Hospital of Psychiatry, Zurich, Switzerland

* Corresponding author. Email: vladyslav.vyazovskiy@dpag.ox.ac.uk

Funding acknowledgements**:** BBSRC (BB/K011847/1, BB/M011224/1), MRC (MR/L003635/1), Wellcome Trust (098461/Z/12/Z), John Fell OUP Research Fund (131/032).

The authors declare no competing interests, financial or otherwise.

Abstract

The homeostatic regulation of sleep manifests as a relative constancy of its daily amount and intensity. Theoretical descriptions of this phenomenon define "Process S", a variable with dynamics dependent only on sleep-wake history, whose levels are reflected in electroencephalogram (EEG) slow wave activity (0.5 – 4 Hz) during sleep. Here we developed novel mathematical models of Process S in mice, assuming that its dynamics are a function of the deviation of cortical neuronal firing rates from a locally defined set-point, crucially without explicit knowledge of sleep-wake state. Our results suggest that Process S tracks global sleep-wake history through an integration of local cortical neuronal activity levels over time. We posit that, instead of reflecting sleep-wake-dependent changes in specific variables and serving their homeostatic regulation, Process S may be a time-keeping mechanism which enables individuals to obtain a species-specific and ecologically-relevant quantity of sleep, even in the absence of external temporal information.

Introduction

According to traditional theory, the need for sleep accumulates during wakefulness and dissipates during sleep. Despite decades of research, it is still uncertain precisely which biological variables form the substrate of sleep need, what characteristics of wake challenge their stability, how information about sleep-wake history is integrated over time, and how sleep mediates the restoration of homeostasis. Daily sleep amount varies greatly across the animal kingdom, yet individuals generally perform a relatively constant and species-specific amount of sleep each day. An even more fundamental question therefore remains whether homeostatic sleep regulation reflects an active process, dynamically shaping daily sleep architecture in response to a physiological need for the homeostatic regulation of specific variables, or whether it corresponds instead to an unknown innate time-keeping process which ensures only that a certain daily quota of sleep is obtained.

The earliest theories of sleep homeostasis supposed the existence of a single variable, termed Process S, which describes sleep drive at the global level (Borbély, 1982). This variable is assumed to always increase during wakefulness, independently of its content, and to decline during sleep. It is widely acknowledged that homeostatic sleep pressure is reflected in the levels of slow wave activity (SWA, 0.5-

4 Hz spectral power) observable during NREM sleep in neurophysiological field potentials, such as electroencephalogram (EEG) or local field potential (LFP).

Current views on the origin of sleep homeostasis emphasise its local and activity-dependent component (Krueger & Tononi, 2011; Rattenborg et al., 2012; Tononi & Cirelli, 2014). It was shown that SWA is far from uniform across the brain, and that the behavioural and cognitive content of waking, beyond its mere duration, influences subsequent sleep and SWA (Kattler et al., 1994; Huber et al., 2004; Vyazovskiy & Tobler, 2008; Rector et al., 2009; Murphy et al. 2011; Fisher et al., 2016). Indeed, many candidate mechanisms for the substrate of sleep homeostasis implicate processes occurring at a cellular and network level. These include the maintenance of cellular homeostasis (Reimund 1994; Mackiewicz et al., 2007; Vyazovskiy & Harris, 2013; Bellesi et al., 2016), the replenishment of energy stores (Scharf et al., 2008), the influence of sleep-related signalling molecules such as adenosine or cytokines (Krueger et al., 2008), and the regulation of imbalanced synaptic strength (Tononi & Cirelli 2003; Vyazovskiy et al., 2008; Liu et al., 2010). Although the equivalence of these processes with Process S has not been conclusively demonstrated (Frank & Heller, 2019), the existing evidence supports the relevance of sleep-wake-dependent differences in neuronal activity for understanding the regulation of sleep.

Cortical neuronal activity is generally higher during waking compared to sleep (Vyazovskiy et al., 2009; Hengen et al., 2016; McKillop et al., 2018). Lower spike firing typical of sleep is due, at least in part, to regular periods of widespread synchronous network silence, termed off periods, intruding on ongoing activity (Steriade et al., 1993a; Steriade et al., 2001; Sanchez-Vives & Mattia, 2014). Importantly, off periods in neural populations are thought to underpin slow wave dynamics at the level of the field potential (Steriade et al., 1993b; Massimini et al., 2004; Buzsáki et al., 2012) and their properties reflect homeostatic sleep need (Vyazovskiy et al., 2009; McKillop et al., 2018; Saberi-Moghadam et al., 2018).

Neuronal firing rates typically fluctuate around a homeostatic set point, which is characteristic for individual cells and variable across the population (Turrigiano, 2011; Hengen et al., 2013; O'Leary et al., 2014; Styr et al., 2019). The homeostatic regulation of firing rates may depend on processes occurring specifically in sleep and wakefulness (Grosmark et al., 2012; Hengen et al, 2016) and evidence suggests that firing rates change as a function of time spent awake, conditional on the behaviour (Vyazovskiy et

68 al., 2009; Fisher et al., 2016). Additionally, the magnitude and direction of state-dependent changes in
69 firing rate differs between neurons, depending on the brain region and their individual firing rate set
70 point (Miyawaki & Diba 2016; Watson et al., 2016; Miyawaki et al., 2019). Firing rate homeostasis may
71 occur above the individual cell level (Slomowitz et al., 2015), perhaps through synaptic plasticity
72 induced by the sleep slow oscillation which may act to narrow the population firing rate distribution
73 (Levenstein et al., 2017).

74 Overall, the evidence suggests that the homeostatic regulation of sleep and of neuronal firing rates may
75 be intrinsically related, however, this functional link remains incompletely defined. Mathematical
76 modelling approaches present an opportunity to address this problem. To this end, we developed novel
77 quantitative models of Process S and demonstrated that its temporal dynamics, on both a local and
78 global level, can be derived entirely from local neuronal activity, without any reference to the animal's
79 sleep and wake states. We found that the magnitude of the deviation of multi-unit firing rate from a
80 locally specified set point carries sufficient information to account for empirically derived patterns of
81 SWA. We then introduced the total time spent in off periods as an alternative measure for Process S with
82 more local origins than SWA, and showed how Process S dynamics may then be described in terms of
83 two opponent processes, dependent on spiking rate and off period occurrence. Our data show that the
84 global dynamics of Process S can be derived from a spatiotemporal integration of local neuronal
85 activities. This suggests that a possible functional role for sleep homeostasis is to provide a precise
86 intrinsic time-keeping mechanism, ensuring that individuals may obtain a species-specific daily quota
87 of sleep even in the absence of external time cues.

88 **Materials & Methods**

89 **Animals, surgery & husbandry**

90 Chronic electrophysiological recordings from six male young adult (4.8 – 5.7 months old, mean 5.2
91 months) C57BL/6J mice were analysed here. This data set is a subset of that used in a previous study
92 (McKillop et al., 2018). The animals were surgically implanted with electrodes for the continuous
93 recording of electroencephalography, electromyography and cortical neuronal activity. EEG screw
94 electrodes (Fine Science Tools) were inserted into the skull above the frontal cortex (primary motor

area: anteroposterior 2mm, mediolateral 2mm) and occipital cortex (primary visual area: anteroposterior 3.5mm, mediolateral 2.5mm). Additional screw electrodes were placed contralateral to the occipital screw and above the cerebellum to serve as the ground and reference electrodes, respectively. A pair of stainless steel wires were inserted into the nuchal muscle for the recording of electromyogram (EMG). A polyimide-insulated tungsten microwire array (Tucker-Davis Technologies) was implanted through a craniotomy window into the frontal cortex (primary motor area: anteroposterior 2mm, mediolateral -2mm), contralateral to the EEG screw. The array comprised 16 wire channels of 33μm diameter, arranged in 2 rows of 8, with columnar separation of 250μm, row separation of 375μm and tip angle of 45 degrees. One row of wires was 250μm longer than the other to account for cortical curvature. A silicone gel (KwikSil, World Precision Instruments) was used to seal the craniotomy, and dental acrylic cement used to stabilise all the implanted electrodes. Surgeries were performed under isoflurane anaesthesia (4% induction, 1-2% maintenance). Analgesics were given immediately before surgery (1-2 mg/kg metacam and 0.08 mg/kg vetergesic, subcutaneous injection) and for at least 3 days during recovery following surgery (1-2 mg/kg metacam, oral). In addition, an immunosuppressant (0.2 mg/kg dexamethasone) was given the day before surgery, immediately before surgery and during recovery for at least 2 days. Animal wellbeing was closely monitored during recovery until a stable return to baseline was observed. All procedures were performed under a UK Home Office Project License and conformed to the Animal (Scientific Procedures) Act 1986.

Mice were housed individually following surgery. Two weeks after surgery, mice were transferred, still individually, to custom made Plexiglas cages (20.3x32x35 cm), containing a running wheel (Campden Instruments), which were placed within ventilated sound-attenuated Faraday chambers (Campden Instruments). The animals were exposed to a standard 12h-12h light dark cycle, with food and water available *ad libitum*. Mice were allowed to habituate to the recording chamber and to attachment of the recording cables for a minimum of three days.

Experimental design

All the data analysed here were collected over two days. The first day served as a baseline, while the animals were completely undisturbed. A sleep deprivation protocol was enforced at light onset on the

second day, immediately after the baseline day, and lasted 6 hours. Sleep deprivation was performed using the well-established gentle handling procedure (Fisher et al., 2016). During this period, experimenters constantly monitored both the behaviour and ongoing neurophysiological recordings of the mice. As soon as any animal showed signs of sleepiness (such as immobility, or slow waves in the EEG), novel objects were introduced to the cage (such as cardboard, colourful plastic and tissue paper) in order to encourage wakefulness. During the sleep deprivation period of 6 h, these mice slept 6.1 ± 2.9 min (mean ± sd) only.

Data collection & pre-processing

Data acquisition was performed using a Multichannel Neurophysiology Recording System (Tucker Davis Technologies). EEG, EMG and microwire array LFP signals were filtered (0.1-100 Hz), amplified (PZ5 NeuroDigitizer preamplifier, TDT) and stored locally (256.9 Hz sampling rate). Custom written Matlab scripts were used for signal conversion and data pre-processing. The LFP, EMG and EEG signals were filtered again offline between 0.5 - 100 Hz (4th order Type II Chebyshev filter) and resampled at 256 Hz.

Extracellular multi-unit spiking was additionally obtained from each microwire array channel, recorded at 25 kHz and filtered 300 Hz – 5 kHz. An amplitude threshold (at least 2 standard deviations, minimum -25 μV) was used to identify putative spikes. Individual spikes were saved as a voltage waveform comprising 46 data samples (0.48 ms before to 1.36 ms after threshold crossing) plus a time stamp of occurrence. Spiking activity from each channel was cleaned offline for artefacts using the Matlab spike sorting software Wave_clus (Quiroga et al., 2004). All putative single unit clusters identified by the algorithm from the same channel were merged, excluding only noise spikes. MUA firing rate for each channel was calculated in epochs of 4 s and expressed in Hz.

Vigilance states were scored manually by visual inspection at a resolution of 4 s (using the software SleepSign, Kissei Comtec). Vigilance states were classified as waking (low amplitude but high frequency EEG with high or phasic EMG activity), NREM sleep (presence of EEG slow waves, a signal of a high amplitude and low frequency, and a low level of EMG activity) or REM sleep (low amplitude, high frequency EEG, and low EMG). For this analysis, over the six mice, a total of 78 out of 96 channels could be analysed (minimum of 10 out of 16 from one mouse). The excluded channels were characterised by

149 an unstable MUA firing rate, including a large drift in firing which was persistent and sleep-wake state
150 independent. For the off occupancy models described below, 75 out of 96 channels were used; a further
151 3 channels had to be excluded because multi-unit firing rates, while stable, were too low to yield a
152 reasonable estimate of the occurrence of off periods.

153 **Slow wave activity**

154 Each EEG and LFP signal was processed to extract a measure of the slow wave activity (SWA). Signal
155 segments were extracted within windows of 4-s duration and 1-s spacing (giving 3-s overlap), and Hann
156 tapered. A Fourier transform was applied to each signal segment and the mean power in the slow wave
157 range (frequencies from 0.5 to 4 Hz) was calculated. This measure was smoothed by finding the median
158 over five temporally adjacent overlapping segments, yielding a SWA measurement for each sequential
159 epoch of 4 s. For normalisation within each channel, SWA values were then expressed as a percentage
160 of the mean SWA calculated over all artefact-free epochs scored as NREM sleep in the baseline 24 hours.
161 The median value of the SWA during each continuous NREM sleep episode served as an estimate of
162 Process S. NREM sleep episodes shorter than 1 min (15 epochs) were excluded, as in a previous study
163 modelling Process S in mice (Guillaumin et al., 2018). Brief awakenings (short arousals accompanied by
164 movement, lasting <20 s) were excluded from analysis but were not considered to be the ending of a
165 NREM sleep episode.

166 **Off period detection and definition of "off occupancy"**

167 One aim of this study was to develop measures of Process S independent of the EEG, and so we focused
168 on off periods which are the neuronal counterpart of slow waves. Off periods refer to brief interruptions
169 of spiking activity which occur synchronously across many recording sites, last approximately 70-100
170 ms (Vyazovskiy et al., 2009), and are coincident with the positive deflection of LFP slow waves (McKillop
171 et al., 2018). In these studies, off periods were detected by pooling spikes over all channels and
172 identifying inter-spike intervals (ISIs) that exceed a threshold duration. However, pooling spikes
173 removes the ability to compare local differences, and if an off period does not involve all channels it will
174 go undetected. To overcome this limitation, off periods were defined separately for each channel by
175 looking at the co-occurrence of local slow waves and spiking silence.

There is no universally accepted method for slow wave detection, and a recent comparison suggests that a simple amplitude-threshold-based approach, while in theory adequate, may underperform due to channel differences in overall LFP amplitude and large amplitude fluctuations of higher frequencies (Bukhtiyarova et al., 2019). For this reason, the LFP was first filtered from 0.5 to 6 Hz (4th order Butterworth filter), and a threshold defined individually for each channel, using the median plus one median absolute deviation of the peak amplitude of all positive half waves (including all vigilance states, but excluding epochs with artefacts). All positive half waves with peak amplitude above threshold were then considered to be slow waves.

Next, for each LFP slow wave, the multi-unit spike preceding and following the slow wave peak was identified and the corresponding ISI determined. The distribution of these ISIs which coincide with slow waves was often (in 64 out of 75 channels) unambiguously bimodal, allowing the threshold to be selected at the local minimum between these two modes. When there was no evidence of bimodality a value of 120 ms was chosen, corresponding to the maximum value selected for the other channels. All inter-spike intervals aligned to slow wave peaks with duration exceeding the threshold were considered off periods. Finally, the metric termed off occupancy was defined, for each epoch of 4 s, as the percentage of time spent in a detected off period during that epoch. Just as with SWA (see above), the median value of off occupancy over NREM sleep episodes was used to represent the level of Process S.

Model fitting and parameter optimisation

Three theoretical models were used to describe the time course of Process S (see Results). The model equations were solved using a discrete time approximation, iteratively updating the value of modelled Process S in time steps of 4 s (Euler method). The fitting of various models to a particular channel of data is equivalent to finding the optimal choice of parameters to achieve the closest match between simulation and empirical SWA/off occupancy. In all models, the initial value of Process S was included as an additional free parameter. The selection of parameter values for model fitting was achieved using a semi-automated approach. First, an algorithmic methodology was established, which depends primarily on the definition of an error metric to assess fit quality between modelled Process S and empirical data. For each animal, NREM sleep episodes were identified with a duration of at least 1

minute. For each NREM sleep episode (***n=1:N***), the median empirical SWA/off occupancy (***X_n***), and similarly the median modelled value of Process S (***S_n***), were computed. The error metric (***E***) is defined as the sum of absolute differences between model and data, weighted by the relative episode duration (***w_n***). This weight was defined as the absolute duration (***d_n***) of the NREM sleep episode, normalised by the total duration of all episodes.

$$E = \sum_{n=1:N} w_n . |X_n - S_n|$$

$$w_n = d_n / \sum_{i=1:N} d_i$$

Algorithmic parameter optimisation was performed separately for each channel, aiming to minimise this error metric. This was achieved using the Matlab function *fminsearch*, which uses the Nelder-Mead simplex algorithm (Lagarias et al., 1998). Many parameter combinations produce very similar dynamics, and many possible optimal (or near-optimal) parameter regimes exist, therefore algorithmic optimisation is sensitive to initial values. For this reason, initial values for the parameters were first set manually, aided with the use of a custom-made Matlab graphical user interface. Manually selected values were then fed into the algorithmic optimisation. Final parameter values were visually inspected to ensure that this optimisation produced an improvement of fit.

The final fit quality of a model to the data was expressed as the median percent error (***E****). This is calculated by finding the absolute difference between median empirical (***X_n***) and simulated (***S_n***) SWA/off occupancy for each NREM sleep episode, expressed as a percentage of the empirical SWA/off occupancy in that episode. ***E**** is then defined as the median over all NREM sleep episodes of these difference values. This alternative error metric is used for presentation of results because it has more comprehensible units (percentage of empirical SWA/off occupancy) compared to the error metric, with arbitrary units.

$$E^* = \underset{n=1:N}{\text{median}} \left[\frac{|X_n - S_n|}{X_n} . 100\% \right]$$

Statistical analyses

The correlation between wake duration, wake firing rates and changes in SWA was calculated separately for each LFP channel. We first identified episodes of NREM sleep of at least 1-minute duration (exactly

228 as for modelling) and obtained the median SWA in each episode. We then identified which intervening
229 time periods, between two NREM episodes, comprised at least 80% wake and lasted at least 5 minutes.
230 We then calculated Pearson correlation coefficients between i) the duration of these wake periods, ii)
231 the mean multi-unit firing rate during these periods, and iii) the change in median SWA from preceding
232 to the following NREM sleep episode.

233 Analysis of variance was performed to explore factors influencing model parameters and fit quality
234 using the Matlab functions *anova1* (one-way) and *anovan* (two-way with unequal group size). For the
235 rate parameters, ANOVA was calculated after applying a log transform. The effect size ($\boldsymbol{\eta^2}$) is calculated
236 for a factor as its sum of squares divided by the total sum of squares in the ANOVA and reflects the
237 fraction of the variance accounted for by that factor.

238 To summarise the results in figures, boxplots were included alongside individual data points. These
239 indicate the median, 25th and 75th percentiles, with whiskers extending to the most extreme value which
240 falls within 150 % of the interquartile range of the box. For these plots, results from individual channels
241 were typically pooled across animals. In some cases, where indicated, channels from the same animal
242 were presented as separate populations.

243 **Results**

244 We selected a dataset of chronic recordings of frontal electroencephalogram (EEG) alongside local field
245 potential (LFP) and multi-unit activity (MUA) spiking from primary motor cortex from six mice. These
246 recordings were made continuously over 48 hours, starting at light onset, while the mice were freely
247 behaving within their cage and exposed to a standard 12hr-12hr light-dark cycle. At light onset of the
248 second day a sleep deprivation protocol was enforced for 6 hours, involving the presentation of novel
249 objects. Outside of this sleep deprivation period, mice were undisturbed and able to sleep at will.

250 **Process S dynamics can be described as a function of vigilance state history**

251 NREM sleep can be defined and distinguished from waking by the presence of high amplitude slow (0.5
252 - 4Hz) waves in the EEG. The average EEG spectral power in the slow wave range (termed slow wave
253 activity; SWA) in NREM sleep varies as a function of the animal's recent sleep-wake history, and this

relationship has been captured in a classical quantitative theory using the concept of "Process S" (Borbély, 1982; Daan et al., 1984). Process S describes a variable whose magnitude can be estimated using the level of SWA during NREM sleep, reflecting the intensity of sleep, and which is interpreted as corresponding to the homeostatic component of sleep drive (Franken et al., 1991a; Achermann et al., 1993; Huber et al., 2000a; Vyazovskiy et al., 2007; Guillaumin et al., 2018). Theoretically, Process S follows simple dynamics: during wake it increases according to a saturating exponential function towards an upper asymptote, while during NREM sleep it decays exponentially towards a lower asymptote. There are many published variants of the precise equations for this model, but crucially, all these variants use the sleep-wake state history of the animal as the key predictive variable for Process S. Here, the specific equations used are:

$$\text{Wake/REM Sleep:} \quad {dS}/{dt} = \alpha(S_{max} - S(t))$$

$$\text{NREM Sleep:} \quad {dS}/{dt} = -\beta(S(t) - S_{min})$$

Where $\boldsymbol{S}$ represents the level of Process S, $\boldsymbol{S_{max}}$ and $\boldsymbol{S_{min}}$ are upper and lower asymptotes, and $\boldsymbol{\alpha}$ and $\boldsymbol{\beta}$ are rate parameters. The first equation is applied when the animal is scored to be awake or in REM sleep and the second equation is applied when it is scored to be in NREM sleep. Here, we use the typical approach of applying the wake dynamics equation to REM sleep (Franken et al., 1991a; Huber et al., 2000a; Vyazovskiy et al.; 2007), but for simplicity do not set separate parameters for wake vs. REM sleep. For convenience, $\boldsymbol{S}$ is expressed in units equivalent to those of SWA. This classical formalism is later abbreviated as model Cl-SWA. Process S as described by these simple dynamics accounts for the time course of empirical SWA with high accuracy. We applied this model to SWA derived from the frontal EEG of all animals, and as expected obtained a high quality fit (Figure 1A).

Neuronal firing rates are associated with Process S dynamics and vigilance state distributions

Whichever specific processes within the brain underpin these state-dependent dynamics for Process S, we hypothesised that it is associated in some way to neuronal spiking activity, which differs characteristically between wake and NREM sleep (Figure 1B). The occurrence of spiking off periods causes firing rates to be typically much lower during NREM sleep compared to wake and REM sleep. Consistent with this assumption, we found that the mean multi-unit firing rate averaged over all periods

of wake was larger than the firing rate averaged over all periods of NREM sleep in every recording channel and every animal in this dataset (Figure 1C).

Because the slow oscillation is underpinned by local neuronal dynamics, it is expected to be highly heterogeneous across the neocortex. Regional differences in SWA dynamics have been previously described, for example between frontal and occipital EEG derivations (Werth et al., 1996; Huber et al., 2000b), and can be accounted for within the classical Process S model through the selection of locally variable values for model rate parameters (Zavada et al., 2009; Rusterholz & Achermann, 2011; Guillaumin et al., 2018). To explore whether spike firing rates might account for some of the variation in the rate of increase of Process S, we correlated the change in LFP SWA from one NREM sleep episode to the next, when separated by wakefulness lasting at least 5 minutes, with the mean spike firing rate during this intervening wake period, and with the duration of that wake period. Correlation coefficients were obtained separately for each recording channel, and pooled across animals. As expected, we obtained large positive correlation coefficients between the duration of a period of wakefulness and the change in LFP SWA in all channels (mean=0.66, sd=0.13; Figure 1D). Importantly however, the change in LFP SWA was on average also positively correlated with the firing rate (mean=0.27, sd=0.30; Figure 1D,E), meaning that, generally, a higher firing rate during waking was associated with a larger increase in SWA in subsequent NREM sleep. Interestingly, these phenomena were not independent, as a positive correlation was also found between wake episode duration and firing rate (mean=0.35, sd= 0.33; Figure 1D). These results further support the possibility that neuronal activity is associated with Process S dynamics. To test this hypothesis we next turned to a quantitative modelling approach.

Process S dynamics can be described as a function of neuronal firing rates

We first sought to determine whether a model expressing Process S dynamics solely as a function of local multi-unit neuronal firing rates might describe the levels of sleep SWA in the corresponding LFP with comparable accuracy to the classical model which is dependent on vigilance states defined at the global level. The classical Process S model was used as a starting point for the development of a novel firing-rate-dependent alternative. To do this, the equations of the classical model were adapted in two ways. Firstly, an instantaneous firing rate threshold ($\boldsymbol{F_\theta}$) was introduced as a new model parameter to

replace the wake vs. sleep criterion, assuming an increase in Process S when the threshold is exceeded and decrease when firing is below. Conceptually, this firing rate threshold resembles a set point; a target firing rate at which the dynamics are stable. Secondly, we assumed that the rate of change of Process S is proportional to the difference between firing rate and this threshold. Introducing this change to the equations ensures that the rate of change of $\boldsymbol{S}$ is equal to zero exactly at the set point, and a continuous function of firing rate around this value. This version of the model is later abbreviated as Fr-SWA. The equations are:

$$F(t) > F_\theta: \quad {dS}/{dt} = \alpha(S_{max} - S(t))(F(t) - F_\theta)$$

$$F(t) < F_\theta: \quad {dS}/{dt} = -\beta(S(t) - S_{min})(F_\theta - F(t))$$

$$F(t) = F_\theta: \quad {dS}/{dt} = 0$$

We applied this novel model, alongside the classical model, to describe SWA dynamics at the LFP level, by finding parameter values that would minimise the difference between empirical SWA and modelled Process S. The two models were fit to the SWA from each LFP channel separately, using the multi-unit firing rate from the same channel for the firing-rate-dependent model. The models were also fit to the SWA obtained by averaging the LFP (and firing rate) over the whole population of channels within the same mouse.

Figure 2 shows two examples of the fit of both models, first to SWA derived from the average LFP, and also to SWA derived from a single LFP channel (these examples are from the same animal as in Figure 1A). The overall pattern of Process S dynamics was similar at both LFP and EEG recording levels and was well described by both the classic and novel firing-rate-based model. Throughout the dataset, this purely firing-rate-dependent model described the overall dynamics of LFP SWA during NREM sleep to a comparable accuracy as the classical model, as reflected in the median percent error deviation between modelled and empirical SWA (Figure 3B). Both the model type and animal have a highly significant effect on the median percent error of the model fit to individual LFP channels, although there is no significant interaction (Model: $F_{(1, 144)} = 25.9$, $p = 1.1\text{x}10^{-6}$; Animal: $F_{(5, 144)} = 30.2$, $p = 6.3\text{x}10^{-21}$; Model x Animal: $F_{(5, 144)} = 1.65$, $p = 0.15$; two-way ANOVA unequal groups). Errors were higher for the novel model, importantly however, the differences in fit quality due to the model type are small relative

330 to the effect size of the particular animal and channel, on which fit quality depends much more strongly
331 (Model: $\eta^2 = 0.079$; Animal: $\eta^2 = 0.459$; Model x Animal: $\eta^2 = 0.025$; Channel (residuals): $\eta^2 = 0.437$). The
332 errors of the model fit on the averaged LFP and on the EEG (classical model only) are also shown in
333 Figure 3B, and are more explicitly compared in Figure 3C. We do not find any significant effect of the
334 field potential level (EEG, average LFP, single LFP channels) on the model error ($F_{(2,171)} = 0.2$, $p = 0.82$,
335 one-way ANOVA).

336 The distributions of final optimised parameters are shown in Figure 3D-G for the classic model and
337 Figure 3H-L for the firing-rate-based model. Most parameters in both models were significantly
338 different between animals, with the exception of $\boldsymbol{S_{min}}$ in the firing-rate-dependent model (Cl-SWA $\boldsymbol{\alpha}$:
339 $F_{(5,77)} = 4.03$, $p = 2.8\text{x}10^{-3}$; Cl-SWA $\boldsymbol{\beta}$: $F_{(5,77)} = 8.65$, $p = 1.9\text{x}10^{-6}$; Cl-SWA $\boldsymbol{S_{max}}$: $F_{(5,77)} = 14.35$, $p = 9.8\text{x}10^{-10}$;
340 Cl-SWA $\boldsymbol{S_{min}}$: $F_{(5,77)} = 12.42$, $p = 1.1\text{x}10^{-8}$; Fr-SWA $\boldsymbol{\alpha}$: $F_{(5,77)} = 8.33$, $p = 3.0\text{x}10^{-6}$; Fr-SWA $\boldsymbol{\beta}$: $F_{(5,77)} = 9.27$, p
341 $= 7.5\text{x}10^{-7}$; Fr-SWA $\boldsymbol{F_\theta}$: $F_{(5,77)} = 14.3$, $p = 1.0\text{x}10^{-9}$; Fr-SWA $\boldsymbol{S_{max}}$: $F_{(5,77)} = 6.64$, $p = 3.9\text{x}10^{-5}$; Fr-SWA $\boldsymbol{S_{min}}$:
342 $F_{(5,77)} = 2.16$, $p = 0.07$; one way ANOVA). The optimised rate parameters for EEG and averaged LFP data
343 consistently fall within the range of the single channel population (Figure 3D-L). The relationship
344 between the optimal firing set point and state specific firing rates is shown in Figure 3M. Firing rate
345 threshold was z-normalised (subtract the mean firing rate over a given state and divide by the standard
346 deviation) separately with respect to the distribution of firing rates in wake, NREM and REM sleep. This
347 shows, as expected, that the set point is typically below mean firing in wake (-1.0 ± 0.6; mean ± sd), well
348 above mean firing in NREM sleep (1.6 ± 1.1), and slightly above mean firing of REM sleep (0.7 ± 1.1).
349 These were all significantly different from zero (wake: $p = 1.6\text{x}10^{-13}$, NREM: $p = 1.9\text{x}10^{-14}$, REM: p =
350 $3.4\text{x}10^{-7}$, two-sided Wilcoxon signed rank test). Figure 3N further shows the state-dependent
351 distribution of average firing rate, expressed as a percentage of the chosen firing set point parameter.
352 Mean firing was 182 ± 57.6% of the firing rate set point during wake, 61.8 ± 17.6 % during NREM sleep,
353 and 84.2 ± 31.8 % during REM sleep. Again, these distributions were all significantly different from
354 100% (Wake: $p = 6.7\text{x}10^{-14}$, NREM: $p = 2.0\text{x}10^{-14}$, REM: $p = 5.4\text{x}10^{-5}$). Note that, in a few channels, the
355 optimal firing rate threshold is actually above the mean firing rate during waking. This occurs when the
356 waking firing rate distribution overlaps substantially with the NREM sleep firing rate distribution but
357 has a heavier tail. REM sleep, in this dataset, is typically associated with firing below the set point, and

358 therefore Process S decreases, albeit at a reduced rate compared to NREM sleep (Figure 3O).
359 Interestingly, there are no significant correlations between the model fit error and the threshold
360 normalisation relative to any one vigilance state (Wake: p=0.06, r=0.21; NREM: p=0.35, r=-0.11; REM:
361 p=0.94, r=-0.01), suggesting that there is no clear relationship between the firing rate set point and firing
362 rate distribution of any one particular state.

363 **Process S can be defined in terms of neuronal spiking off periods**

364 When considering the relationship between multi-unit firing rates and LFP slow waves, a conceptual
365 complication arises due to the different origins of the LFP and MUA from within the same channel. While
366 the MUA firing rate represents the activity of only a few individual neurones, factors such as volume
367 conduction result in spatial smoothing of the LFP signal, and as such it represents the combined activity
368 of neurones covering a cortical area potentially on the order of several millimetres (Kajikawa &
369 Schroeder, 2011). This means that when a slow wave is detected in the LFP, it is not guaranteed that all
370 local neurones contributing to the MUA are necessarily silent (Todorova & Zugaro, 2019). Similarly, not
371 every long interspike interval occurs during a slow wave. An estimation of the occurrence of off periods
372 may be obtained by combining LFP and spiking data (Figure 4A). Slow wave detection was performed
373 on each LFP over the whole 48 h, including all vigilance states (0.5-6 Hz filter followed by an amplitude
374 threshold, values shown in Figure 4C). All multi-unit inter-spike intervals (ISIs) which coincide with the
375 peak of detected slow waves were identified. The distribution of the duration of these ISIs was often (64
376 out of 75 channels) unambiguously bimodal (Figure 4B). This could be interpreted as evidence of the
377 existence of two spiking states occurring locally during the more widespread network slow oscillation;
378 high frequency spiking (on period) and extended silence (off period). Note that these two distributions
379 do not simply correspond exactly to sleep vs. wake conditions, because bimodality is often evident in
380 the distribution of slow wave coincident ISIs from NREM sleep only, or even from REM sleep only (Figure
381 4B). The distribution of slow wave coincident ISIs (over all vigilance states) was used to define an ISI
382 duration threshold for the detection of off periods, separately for each channel. The values used for this
383 threshold are shown in Figure 4D. The average multi-unit firing rate aligned to the peak of slow waves
384 in detected off periods reveals a clear suppression of firing, consistent with expectations (Figure 4E). A

385 rebound increase in average firing is visible in this example channel immediately after the off period, as
386 has been previously documented in some cortical neuronal populations (Chauvette et al., 2010). The
387 total fraction of time each channel spends in off periods was calculated over all epochs of 4 s, and termed
388 the "off occupancy". Off occupancy defined in this way is high in NREM sleep and low in both wake and
389 REM sleep (Figure 4F). The existence of a non-zero frequency of local cortical off periods has been
390 previously reported during wakefulness (Vyazovskiy et al., 2011; Vyazovskiy et al., 2014; Fisher et al.,
391 2016), and REM sleep (Funk et al., 2016). The off occupancy measure displays similar temporal
392 dynamics to LFP (and EEG) SWA over both sleep deprivation and spontaneous sleep and wake (Figure
393 4G).

394 **Process S dynamics, defined using off periods, can be described as a function of vigilance states**
395 **or neuronal firing rates**

396 In order to investigate whether the off occupancy measure reflects Process S, we applied the classical
397 state-based model to the time course of off occupancy, exactly as was done with single channel SWA.
398 The classical model was applied with its equations unchanged, and is abbreviated as Cl-Off. Figure 5A
399 shows an example of the resulting Process S time course obtained in this way with a high quality of fit.
400 In contrast, some changes were introduced to the firing-rate-based model in order to describe off
401 occupancy dynamics. We considered that the different dynamics above vs. below a particular firing rate
402 set point may be due to two opponent processes simultaneously active in dynamic opposition but with
403 differential magnitude in wake vs. NREM sleep. Specifically, we consider a Process S increasing term
404 which is proportional to instantaneous firing rate, and a Process S decreasing term which is proportional
405 to the time spent in off periods (off occupancy). The equation used is:

406 $$dS/dt = \alpha F(t)\big(S_{max} - S(t)\big) - \beta X(t)(S(t) - S_{min})$$

407 In this model, one term drives $\boldsymbol{S}$ towards an upper asymptote ($\boldsymbol{S_{max}}$) in proportion to firing rate ($\boldsymbol{F}$), while
408 the other drives $\boldsymbol{S}$ towards a lower asymptote ($\boldsymbol{S_{min}}$) in proportion to the off occupancy ($\boldsymbol{X}$). Again, two
409 rate parameters $\boldsymbol{\alpha}$ & $\boldsymbol{\beta}$ are required. This model behaves similarly to previous models because firing is
410 high in wake and low in NREM sleep, whereas off occupancy is high in NREM sleep and low in wake. This

411 variant of the model is abbreviated as Fr-Off. Figure 5A also includes the fit from this model,
412 demonstrating a high level of agreement between the two models and an accurate fit to the data.

413 The distribution of the median percent errors for the fits from both models over all animals and channels
414 is shown in Figure 5C. As before, the model type and animal has a significant effect (Model: $F_{(1,138)} = 8.06$,
415 $p = 5.2\text{x}10^{-3}$; Animal: $F_{(5,138)} = 17.2$, $p = 3.2\text{x}10^{-13}$; Model x Animal: $F_{(5,138)} = 0.52$, $p = 0.76$; two-way ANOVA
416 with unequal groups) and the classic model achieved a slightly lower median percent error. However,
417 this effect was again very weak compared with the variation in fit quality between animals and channels
418 (Model: $\eta^2 = 0.034$; Animal: $\eta^2 = 0.367$; Model x Animal: $\eta^2 = 0.011$; Channel (residuals): $\eta^2 = 0.588$).
419 Figure 5D shows the distribution of values for the change in modelled Process S from one simulated
420 time step to the next resulting from the firing-rate-based model (Fr-Off), in wake, NREM and REM sleep,
421 pooling all animals, channels and time. Unlike in the previous firing-rate-based model, REM sleep is now
422 typically associated with an increase in Process S. The distributions of final optimised parameters are
423 shown in Figure 5E-H for the classic model and Figure 5I-L for the firing rate and off occupancy model.
424 Most parameters in both models were different between animals to a high significance level (Cl-Off $\boldsymbol{\alpha}$:
425 $F_{(5,74)} = 2.4$, $p = 0.047$; Cl-Off $\boldsymbol{\beta}$: $F_{(5,74)} = 2.29$, $p = 0.055$; Cl-Off $\boldsymbol{S_{max}}$: $F_{(5,74)} = 9.49$, $p = 6.4\text{x}10^{-7}$; Cl-Off $\boldsymbol{S_{min}}$:
426 $F_{(5,74)} = 16.79$, $p = 8.0\text{x}10^{-11}$; Fr-Off $\boldsymbol{\alpha}$: $F_{(5,74)} = 9.86$, $p = 3.9\text{x}10^{-7}$; Fr-Off $\boldsymbol{\beta}$: $F_{(5,74)} = 5.14$, $p = 4.6\text{x}10^{-4}$; Fr-Off
427 $\boldsymbol{S_{max}}$: $F_{(5,74)} = 10.08$, $p = 2.8\text{x}10^{-7}$; Fr-Off $\boldsymbol{S_{min}}$: $F_{(5,74)} = 10.25$, $p = 2.3\text{x}10^{-7}$; one way ANOVA). Notably, the
428 weakest evidence for inter-animal differences were for $\boldsymbol{\alpha}$ and $\boldsymbol{\beta}$ in the classic model.

429 **Modelling identifies local variation in Process S dynamics**

430 All four modelling approaches described here suggest the existence of variability in Process S between
431 recording channels, indicating that a local component determines its dynamics. Figure 6A-D illustrates
432 this diversity, showing the overlaid time courses of Process S for all channels within a single
433 representative animal, expressed as a percentage of their individual maximum value for normalisation
434 purposes. Although the models all fit empirical SWA or off period occupancy with generally high
435 accuracy, there are nonetheless differences between models in the precise shape of Process S. The
436 average Process S over all channels was also calculated for each model and compared with the Process
437 S derived from applying the classical model to EEG SWA (Figure 6E). This reveals that Process S derived

438 from modelling LFP SWA more closely resembles Process S derived from EEG SWA than Process S
439 derived from off occupancy. This suggests that global Process S calculated at a higher spatial scale might
440 reflect an averaging across a manifold of local Processes S that exist on a finer spatial level.

441 **Discussion**

442 Here, we demonstrated that Process S dynamics can be derived entirely from neuronal spiking activity,
443 without reference to global sleep-wake states. A model was outlined whereby the integrated history of
444 local multi-unit firing rates, relative to a locally-defined firing rate set point, predicted the temporal
445 dynamics of LFP and global EEG SWA. The accuracy of this model was demonstrated in a dataset of
446 recordings from mouse frontal cortex over 48 hours, including both voluntary sleep and wake, and sleep
447 deprivation. A novel metric for Process S was then presented, termed off occupancy, which measures
448 the fraction of time a neural population spends in off periods, defined by the coincidence of LFP slow
449 waves and multi-unit spiking silence. The modelling approach was combined with the off occupancy
450 metric and tested on the same dataset to present a quantitative framework for understanding dynamics
451 of sleep pressure at a highly local level in terms of neural spiking and off periods.

452 Central to this modelling perspective is the assumption that the generation of spikes by a neural network
453 is in some way correlated with an increase in sleep pressure, and that this manifests in the subsequent
454 expression of slow waves and off periods, reflecting Process S. The energetic cost of spiking is high
455 (Attwell & Laughlin 2001), the regulation of a neurone's firing rate set point is linked to cellular
456 energetics (Styr et al., 2019; Vergara et al., 2019), and neurones are susceptible to cellular stresses that
457 can result from sustained metabolic load, such as oxidative stress (Wang & Michaelis 2010; Cobley et al.,
458 2018; Kempf et al., 2019). Furthermore, spiking activity may be mechanistically associated with synaptic
459 plasticity, and it was suggested that firing rates are an important determinant of overall changes in
460 synaptic strength, with higher spiking leading to greater changes (Graupner et al., 2016; Lappalainen et
461 al., 2019). Compensatory processes exist within neurones to oppose cellular stress and related
462 homeostatic challenges (Kültz 2005) and off periods could provide the opportunity for neurones to
463 prioritise such processes, therefore mediating the restorative benefits of sleep (Vyazovskiy & Harris,
464 2013). Similarly, off periods are associated with distinct synaptic plasticity rules (Gonzalez-Rueda et al.,

465 2018), and so their prevalence and patterning is likely also related to whatever regulation of synaptic
466 strength occurs during sleep (Tononi & Cirelli 2014; Timofeev & Chauvette 2017; Seibt & Frank, 2019).

467 According to this view of sleep homeostasis, in principle, regulation can occur entirely at the local level,
468 within cortical networks or perhaps even within single neurones. Indeed, this is reflected in our results
469 through the differences between channels both with respect to the accuracy of the model and in the
470 values of optimised parameters. Why then is global sleep preferred over a hypothetical state including
471 asynchronous local off periods, which presumably could be used to sustain longer periods of
472 behavioural wakefulness? It has been argued previously that it is ecologically optimal to synchronise off
473 periods and undergo dedicated periods of total behavioural shutdown, because local off periods during
474 waking impair behaviour (Vyazovskiy et al., 2011; Rattenborg et al., 2012). Mechanistically, the
475 occurrence of off periods might be obstructed by strong synaptic coupling and shared neuromodulatory
476 tone. Indeed, it has been observed that the degree of coupling between an individual neurone's firing
477 and the population firing rate, is variable between cells but characteristic to an individual neurone and
478 likely reflects total synaptic strength with its neighbours (Okun et al., 2015). Some neurones may
479 therefore be less able to express asynchronous off periods than others.

480 The preference for global sleep, despite its fundamentally local mechanisms, may be evidence that sleep
481 homeostasis ultimately does not serve a single specific local function. Instead, the recent history of
482 neuronal activity levels may regulate the local tendency to generate off periods (Process S), a signal
483 which is integrated over larger neuronal populations through intrinsic network mechanisms in order to
484 produce a global sleep propensity signal that estimates the total time spent awake with great accuracy.
485 This mechanism would enable the brain to enforce a daily quota of sleep, which could have many
486 benefits at the physiological and ecological level, rather than to initiate sleep in response to the
487 homeostatic need of one specific regulated variable (Vyazovskiy, 2015). Importantly, in this mechanism,
488 the variables which change as a function of time spent awake or asleep do not themselves need to be
489 directly regulated by sleep. Conversely, variables which remain stable during continuous wake or sleep
490 could still make essential contributions to the time-keeping mechanism. Note that this property is
491 present in our model, since the levels of neural activity themselves are not directly proportional to the

492 levels of Process S. The approximately equivalent overall accuracy of both firing-rate-based and
493 vigilance-state-based models supports this possibility, as does the evidence that homeostatically
494 regulated cellular variables can actually be stable during extended wakefulness, and that maintenance
495 processes in sleep may be ultimately prophylactic (Vyazovskiy & Harris, 2013). In order to maximise
496 the efficiency of global sleep, single neuronal activities may be modulated such that sleep pressure
497 accumulates, on average, as uniformly as possible. This is consistent with recent reports that sleep
498 regulates the population level firing rate distribution (Watson et al., 2016; Levenstein et al., 2017;
499 Miyawaki & Diba, 2019) and could account for sleep's link with synaptic and firing rate homeostasis,
500 reconciling the local origins of sleep pressure accumulation with the global level of its dissipation.

501 Here, spike firing rate is used to represent the level of neural activity because it is convenient to record,
502 locally variable, and directly linked to neuronal functionality. However, no strong claim is made that
503 firing rates are necessarily causally responsible for the accumulation of sleep pressure. Indeed, it would
504 likely be possible to obtain a reasonable quantitative account of sleep homeostasis using any
505 physiological variable (or set of variables) that are consistently higher in either the wake or sleep state.
506 For example, a model assuming that Process S increases in proportion to local cortical temperature,
507 which, in laboratory rodents, drops by ~2°C when falling asleep (Franken et al., 1991b; Tobler et al.,
508 1997) and which has been mechanistically implicated in sleep regulation (Hoekstra et al., 2019), might
509 also provide a plausible description of Process S dynamics. However, our results demonstrate that firing
510 rates are a useful measurable correlate of the processes that directly underpin Process S, and therefore
511 firing rate variance resulting from differences in experience and behaviour may well account for the
512 variance in Process S accumulation in normal individuals, between waking periods and between cortical
513 regions.

514 It should be noted that the firing-rate-based models used here typically slightly under-perform, relative
515 to the classic model, in terms of minimising the error between simulation and empirical data. There are
516 a number of reasons why a limit on the accuracy of the model is to be expected, related to technical
517 restrictions rather than conceptual ones. In this approach, each MUA channel records only a few
518 randomly sampled nearby neurones, which may have very different spiking properties, and so grouping

519 these as a single measure of local network activity is somewhat arbitrary. It may be valuable to explore
520 genetic and pharmacological manipulations of firing rate in order to further test this model's validity.
521 Unfortunately, the effects of any manipulation on the accumulation, expression and dissipation of sleep
522 pressure, separately to the effects on firing, is unknown, and so this may be hard to interpret. For
523 example, a recent study found that systemic atropine administered during behavioural wakefulness
524 produces slow wave activity, reducing spiking (as measured by c-Fos) yet increasing the duration of
525 subsequent NREM sleep (Qiu et al., 2015). While this was interpreted as evidence that spiking activity
526 is not related to sleep pressure accumulation, the direct effects of atropine on Process S and the
527 functional significance of the resulting induced slow oscillation are unclear. Similarly, another study
528 found that local optogenetic activation of cortex during sleep, despite raising firing rates to waking
529 levels, was not accompanied with increased SWA or off periods during subsequent NREM sleep
530 (Rodriguez et al., 2016). Again, it is difficult to disentangle the direct effects of this local stimulation,
531 which is not physiologically realistic, on the mechanisms surrounding the accumulation, expression and
532 dissipation of sleep pressure. On the other hand, these results might be interpreted as evidence that the
533 expression of the level of Process S involves an integration of homeostatic sleep need across neural
534 populations and therefore local firing rate manipulations are not able to substantially influence Process
535 S dynamics at a global level.

536 It is reasonable to assume that sleep homeostasis unfolds on multiple time scales and Process S as
537 defined by these models describes a relatively fast one, approaching its upper asymptote after
538 continuous wakefulness on a time scale of hours. The inclusion of processes acting over longer or
539 shorter time scales might explain discrepancies in all these models, however, the challenge remains to
540 identify what these could be. Furthermore, the role of REM sleep in Process S dynamics has not been
541 explicitly addressed or considered in the construction of these models. Depending on the model variant,
542 REM sleep is associated either with a small increase or small decrease in Process S, because firing rates
543 are low in REM sleep (closer to NREM sleep than waking) and yet off period occupancy is also low (closer
544 to wake levels than NREM sleep). It is possible that REM sleep might represent a homeostatically neutral
545 state, in which the level of Process S changes minimally, or not at all (Vyazovskiy & Delogu, 2014).

546 In summary, our data suggest that Process S is reflected at multiple scales in the brain, from EEG and
547 LFP slow wave activity to the occurrence of local multi-unit off periods. Its dynamics across all scales
548 can be described quantitatively using information derived only from local neuronal activity with
549 comparable accuracy to the classical model of Process S which depends on global sleep-wake history.
550 We postulate that, despite its local origins, Process S may be integrated across networks for the purpose
551 of tracking time spent awake and used to enforce a daily quota of global sleep, rather than serving the
552 regulation of specific physiological variables.

References

Achermann, P., Dijk, D.-J., Brunner, D.P., and Borbély, A.A. (1993). A model of human sleep homeostasis based on EEG slow-wave activity: Quantitative comparison of data and simulations. Brain Research Bulletin *31*, 97–113.

Attwell, D., and Laughlin, S.B. (2001). An energy budget for signaling in the grey matter of the brain. J. Cereb. Blood Flow Metab. *21*, 1133–1145.

Bellesi, M., Bushey, D., Chini, M., Tononi, G., and Cirelli, C. (2016). Contribution of sleep to the repair of neuronal DNA double-strand breaks: evidence from flies and mice. Scientific Reports *6*, 36804.

Borbély, A.A. (1982). A two process model of sleep regulation. Hum Neurobiol *1*, 195–204.

Bukhtiyarova, O., Soltani, S., Chauvette, S., and Timofeev, I. (2019). Slow wave detection in sleeping mice: Comparison of traditional and machine learning methods. Journal of Neuroscience Methods *316*, 35–45.

Buzsáki, G., Anastassiou, C.A., and Koch, C. (2012). The origin of extracellular fields and currents — EEG, ECoG, LFP and spikes. Nature Reviews Neuroscience *13*, 407–420.

Chauvette, S., Volgushev, M., and Timofeev, I. (2010). Origin of Active States in Local Neocortical Networks during Slow Sleep Oscillation. Cereb Cortex *20*, 2660–2674.

Cirelli, C., Faraguna, U., and Tononi, G. (2006). Changes in brain gene expression after long-term sleep deprivation. Journal of Neurochemistry *98*, 1632–1645.

Cobley, J.N., Fiorello, M.L., and Bailey, D.M. (2018). 13 reasons why the brain is susceptible to oxidative stress. Redox Biology *15*, 490–503.

Daan, S., Beersma, D.G., and Borbély, A.A. (1984). Timing of human sleep: recovery process gated by a circadian pacemaker. Am. J. Physiol. *246*, R161-183.

Fisher, S.P., Cui, N., McKillop, L.E., Gemignani, J., Bannerman, D.M., Oliver, P.L., Peirson, S.N., and Vyazovskiy, V.V. (2016). Stereotypic wheel running decreases cortical activity in mice. Nature Communications *7*, ncomms13138.

578 Frank, M.G., and Heller, H.C. (2019). The Function(s) of Sleep. Handb Exp Pharmacol.

579 Franken, P., Dijk, D.J., Tobler, I., and Borbély, A.A. (1991a). Sleep deprivation in rats: effects on EEG
580 power spectra, vigilance states, and cortical temperature. American Journal of Physiology-Regulatory,
581 Integrative and Comparative Physiology *261*, R198–R208.

582 Franken, P., Tobler, I., and Borbély, A.A. (1991b). Sleep homeostasis in the rat: simulation of the time
583 course of EEG slow-wave activity. Neurosci. Lett. *130*, 141–144.

584 Funk, C.M., Honjoh, S., Rodriguez, A.V., Cirelli, C., and Tononi, G. (2016). Local Slow Waves in Superficial
585 Layers of Primary Cortical Areas during REM Sleep. Curr. Biol. *26*, 396–403.

586 González-Rueda, A., Pedrosa, V., Feord, R.C., Clopath, C., and Paulsen, O. (2018). Activity-Dependent
587 Downscaling of Subthreshold Synaptic Inputs during Slow-Wave-Sleep-like Activity In Vivo. Neuron
588 *97*, 1244-1252.e5.

589 Graupner, M., Wallisch, P., and Ostojic, S. (2016). Natural Firing Patterns Imply Low Sensitivity of
590 Synaptic Plasticity to Spike Timing Compared with Firing Rate. J Neurosci *36*, 11238–11258.

591 Grosmark, A.D., Mizuseki, K., Pastalkova, E., Diba, K., and Buzsáki, G. (2012). REM Sleep Reorganizes
592 Hippocampal Excitability. Neuron *75*, 1001–1007.

593 Guillaumin, M.C.C., McKillop, L.E., Cui, N., Fisher, S.P., Foster, R.G., de Vos, M., Peirson, S.N., Achermann,
594 P., and Vyazovskiy, V.V. (2018). Cortical region specific sleep homeostasis in mice: effects of time of
595 day and waking experience. Sleep.

596 Hengen, K.B., Lambo, M.E., Van Hooser, S.D., Katz, D.B., and Turrigiano, G.G. (2013). Firing Rate
597 Homeostasis in Visual Cortex of Freely Behaving Rodents. Neuron *80*, 335–342.

598 Hengen, K.B., Pacheco, A.T., McGregor, J.N., Van Hooser, S.D., and Turrigiano, G.G. (2016). Neuronal
599 firing rate homeostasis is inhibited by sleep and promoted by wake. Cell *165*, 180–191.

600 Hoekstra, M.M., Emmenegger, Y., Hubbard, J., and Franken, P. (2019). Cold-inducible RNA-binding
601 protein (CIRBP) adjusts clock-gene expression and REM-sleep recovery following sleep deprivation.
602 ELife *8*.

Huber, R., Deboer, T., and Tobler, I. (2000a). Effects of sleep deprivation on sleep and sleep EEG in three mouse strains: empirical data and simulations. Brain Res. *857*, 8–19.

Huber, R., Deboer, T., and Tobler, I. (2000b). Topography of EEG dynamics after sleep deprivation in mice. J. Neurophysiol. *84*, 1888–1893.

Huber, R., Ghilardi, M.F., Massimini, M., and Tononi, G. (2004). Local sleep and learning. Nature *430*, 78–81.

Kajikawa, Y., and Schroeder, C.E. (2011). How local is the local field potential? Neuron *72*, 847–858.

Kattler, H., Dijk, D.J., and Borbély, A.A. (1994). Effect of unilateral somatosensory stimulation prior to sleep on the sleep EEG in humans. J Sleep Res *3*, 159–164.

Kempf, A., Song, S.M., Talbot, C.B., and Miesenböck, G. (2019). A potassium channel β-subunit couples mitochondrial electron transport to sleep. Nature *568*, 230–234.

Krueger, J.M., and Tononi, G. (2011). Local Use-Dependent Sleep; Synthesis of the New Paradigm. Curr Top Med Chem *11*, 2490–2492.

Krueger, J.M., Rector, D.M., Roy, S., Dongen, H.P.A.V., Belenky, G., and Panksepp, J. (2008). Sleep as a fundamental property of neuronal assemblies. Nature Reviews Neuroscience *9*, 910.

Kültz, D. (2005). Molecular and Evolutionary Basis of the Cellular Stress Response. Annual Review of Physiology *67*, 225–257.

Lagarias, J., Reeds, J., Wright, M., and Wright, P. (1998). Convergence Properties of the Nelder--Mead Simplex Method in Low Dimensions. SIAM J. Optim. *9*, 112–147.

Lappalainen, J., Herpich, J., and Tetzlaff, C. (2019). A Theoretical Framework to Derive Simple, Firing-Rate-Dependent Mathematical Models of Synaptic Plasticity. Front. Comput. Neurosci. *13*.

Levenstein, D., Watson, B.O., Rinzel, J., and Buzsáki, G. (2017). Sleep regulation of the distribution of cortical firing rates. Current Opinion in Neurobiology *44*, 34–42.

626 Liu, Z.-W., Faraguna, U., Cirelli, C., Tononi, G., and Gao, X.-B. (2010). Direct evidence for wake-related
627 increases and sleep-related decreases in synaptic strength in rodent cortex. J. Neurosci. *30*, 8671–
628 8675.

629 Mackiewicz, M., Shockley, K.R., Romer, M.A., Galante, R.J., Zimmerman, J.E., Naidoo, N., Baldwin, D.A.,
630 Jensen, S.T., Churchill, G.A., and Pack, A.I. (2007). Macromolecule biosynthesis: a key function of sleep.
631 Physiol. Genomics *31*, 441–457.

632 Massimini, M., Huber, R., Ferrarelli, F., Hill, S., and Tononi, G. (2004). The sleep slow oscillation as a
633 traveling wave. J. Neurosci. *24*, 6862–6870.

634 McKillop, L.E., Fisher, S.P., Cui, N., Peirson, S.N., Foster, R.G., Wafford, K.A., and Vyazovskiy, V.V. (2018).
635 Effects of Aging on Cortical Neural Dynamics and Local Sleep Homeostasis in Mice. J. Neurosci. *38*,
636 3911–3928.

637 Miyawaki, H., and Diba, K. (2016). Regulation of hippocampal firing by network oscillations during
638 sleep. Curr Biol *26*, 893–902.

639 Miyawaki, H., Watson, B.O., and Diba, K. (2019). Neuronal firing rates diverge during REM and
640 homogenize during non-REM. Scientific Reports *9*, 689.

641 Murphy, M., Huber, R., Esser, S., Riedner, B.A., Massimini, M., Ferrarelli, F., Ghilardi, M.F., and Tononi, G.
642 (2011). The cortical topography of local sleep. Curr Top Med Chem *11*, 2438–2446.

643 Okun, M., Steinmetz, N.A., Cossell, L., Iacaruso, M.F., Ko, H., Barthó, P., Moore, T., Hofer, S.B., Mrsic-
644 Flogel, T.D., Carandini, M., and Harris, K. (2015). Diverse coupling of neurons to populations in sensory
645 cortex. Nature *521*, 511–515.

646 O'Leary, T., Williams, A.H., Franci, A., and Marder, E. (2014). Cell types, network homeostasis, and
647 pathological compensation from a biologically plausible ion channel expression model. Neuron *82*,
648 809–821.

649 Qiu, M.-H., Chen, M.C., and Lu, J. (2015). Cortical neuronal activity does not regulate sleep homeostasis.
650 Neuroscience *297*, 211–218.

651 Quiroga, R.Q., Nadasdy, Z., and Ben-Shaul, Y. (2004). Unsupervised spike detection and sorting with
652 wavelets and superparamagnetic clustering. Neural Comput *16*, 1661–1687.

653 Rattenborg, N.C., Lima, S.L., and Lesku, J.A. (2012). Sleep Locally, Act Globally. Neuroscientist *18*, 533–
654 546.

655 Rector, D.M., Schei, J.L., Van Dongen, H.P.A., Belenky, G., and Krueger, J.M. (2009). Physiological
656 Markers of Local Sleep. Eur J Neurosci *29*, 1771–1778.

657 Reimund, E. (1994). The free radical flux theory of sleep. Medical Hypotheses *43*, 231–233.

658 Rodriguez, A.V., Funk, C.M., Vyazovskiy, V.V., Nir, Y., Tononi, G., and Cirelli, C. (2016). Why Does Sleep
659 Slow-Wave Activity Increase After Extended Wake? Assessing the Effects of Increased Cortical Firing
660 During Wake and Sleep. J. Neurosci. *36*, 12436–12447.

661 Rusterholz, T., and Achermann, P. (2011). Topographical aspects in the dynamics of sleep homeostasis
662 in young men: individual patterns. BMC Neurosci *12*, 84.

663 Saberi-Moghadam, S., Simi, A., Setareh, H., Mikhail, C., and Tafti, M. (2018). In vitro Cortical Network
664 Firing is Homeostatically Regulated: A Model for Sleep Regulation. Sci Rep *8*, 6297.

665 Sanchez-Vives, M., and Mattia, M. (2014). Slow wave activity as the default mode of the cerebral cortex.
666 Archives Italiennes de Biologie *152*, 147–155.

667 Scharf, M.T., Naidoo, N., Zimmerman, J.E., and Pack, A.I. (2008). The energy hypothesis of sleep
668 revisited. Prog. Neurobiol. *86*, 264–280.

669 Seibt, J., and Frank, M.G. (2019). Primed to Sleep: The Dynamics of Synaptic Plasticity Across Brain
670 States. Front Syst Neurosci *13*, 2.

671 Slomowitz, E., Styr, B., Vertkin, I., Milshtein-Parush, H., Nelken, I., Slutsky, M., and Slutsky, I. (2015).
672 Interplay between population firing stability and single neuron dynamics in hippocampal networks.
673 Elife *4*.

674 Steriade, M., Nuñez, A., and Amzica, F. (1993a). A novel slow (< 1 Hz) oscillation of neocortical neurons
675 in vivo: depolarizing and hyperpolarizing components. J. Neurosci. *13*, 3252–3265.

Steriade, M., Nuñez, A., and Amzica, F. (1993b). Intracellular analysis of relations between the slow (< 1 Hz) neocortical oscillation and other sleep rhythms of the electroencephalogram. J. Neurosci. *13*, 3266–3283.

Steriade, M., Timofeev, I., and Grenier, F. (2001). Natural waking and sleep states: a view from inside neocortical neurons. J. Neurophysiol. *85*, 1969–1985.

Styr, B., Gonen, N., Zarhin, D., Ruggiero, A., Atsmon, R., Gazit, N., Braun, G., Frere, S., Vertkin, I., Shapira, I., Harel, H., Heim, L., Katsenelson, M., Rechnitz, O., Fadila, S., Derdikman, D., Rubinstein, M., Geiger, T., Ruppin E., and Slutsky, I. (2019). Mitochondrial Regulation of the Hippocampal Firing Rate Set Point and Seizure Susceptibility. Neuron *102*, 1009-1024.e8.

Timofeev, I., and Chauvette, S. (2017). Sleep slow oscillation and plasticity. Curr. Opin. Neurobiol. *44*, 116–126.

Todorova, R., and Zugaro, M. (2019). Isolated cortical computations during delta waves support memory consolidation. Science *366*, 377–381.

Tobler, I., Deboer, T., and Fischer, M. (1997). Sleep and sleep regulation in normal and prion protein-deficient mice. J. Neurosci. *17*, 1869–1879.

Tononi, G., and Cirelli, C. (2003). Sleep and synaptic homeostasis: a hypothesis. Brain Research Bulletin *62*, 143–150.

Tononi, G., and Cirelli, C. (2014). Sleep and the Price of Plasticity: From Synaptic and Cellular Homeostasis to Memory Consolidation and Integration. Neuron *81*, 12–34.

Turrigiano, G. (2011). Too Many Cooks? Intrinsic and Synaptic Homeostatic Mechanisms in Cortical Circuit Refinement. Annual Review of Neuroscience *34*, 89–103.

Vergara, R.C., Jaramillo-Riveri, S., Luarte, A., Moënne-Loccoz, C., Fuentes, R., Couve, A., and Maldonado, P.E. (2019). The Energy Homeostasis Principle: Neuronal Energy Regulation Drives Local Network Dynamics Generating Behavior. Front Comput Neurosci *13*, 49.

Vyazovskiy, V.V. (2015). Sleep, recovery, and metaregulation: explaining the benefits of sleep. Nat Sci Sleep *7*, 171–184.

Vyazovskiy, V.V., and Delogu, A. (2014). NREM and REM Sleep: Complementary Roles in Recovery after Wakefulness. Neuroscientist *20*, 203–219.

Vyazovskiy, V.V., and Harris, K.D. (2013). Sleep and the single neuron: the role of global slow oscillations in individual cell rest. Nat Rev Neurosci *14*, 443–451.

Vyazovskiy, V.V., and Tobler, I. (2008). Handedness leads to interhemispheric EEG asymmetry during sleep in the rat. J. Neurophysiol. *99*, 969–975.

Vyazovskiy, V.V., Achermann, P., and Tobler, I. (2007). Sleep homeostasis in the rat in the light and dark period. Brain Res. Bull. *74*, 37–44.

Vyazovskiy, V.V., Cirelli, C., Pfister-Genskow, M., Faraguna, U., and Tononi, G. (2008). Molecular and electrophysiological evidence for net synaptic potentiation in wake and depression in sleep. Nat Neurosci *11*, 200–208.

Vyazovskiy, V.V., Olcese, U., Lazimy, Y.M., Faraguna, U., Esser, S.K., Williams, J.C., Cirelli, C., and Tononi, G. (2009). Cortical firing and sleep homeostasis. Neuron *63*, 865–878.

Vyazovskiy, V.V., Olcese, U., Hanlon, E.C., Nir, Y., Cirelli, C., and Tononi, G. (2011). Local sleep in awake rats. Nature *472*, 443–447.

Vyazovskiy, V.V., Cui, N., Rodriguez, A.V., Funk, C., Cirelli, C., and Tononi, G. (2014). The dynamics of cortical neuronal activity in the first minutes after spontaneous awakening in rats and mice. Sleep *37*, 1337–1347.

Wang, X., and Michaelis, E.K. (2010). Selective neuronal vulnerability to oxidative stress in the brain. Front. Aging Neurosci. *2*.

Watson, B.O., Levenstein, D., Greene, J.P., Gelinas, J.N., and Buzsáki, G. (2016). Network Homeostasis and State Dynamics of Neocortical Sleep. ResearchGate.

Werth, E., Achermann, P., and Borbély, A.A. (1996). Brain topography of the human sleep EEG: antero-posterior shifts of spectral power. Neuroreport *8*, 123–127.

Zavada, A., Strijkstra, A.M., Boerema, A.S., Daan, S., and Beersma, D.G.M. (2009). Evidence for differential human slow-wave activity regulation across the brain. J Sleep Res *18*, 3–10.

728 **Figure Legends**

729 **Figure 1.** Cortical spike firing patterns are associated with the dynamics of Process S. **A)** An example of
730 the classical state-based Process S model (blue) describing the dynamics of frontal EEG SWA (median
731 per NREM sleep episode, black bars) over 48 hours in one representative animal. Sleep deprivation
732 occurred as indicated at light onset of the second day and lasted 6 hours. Scored vigilance states are also
733 shown. **B)** An example of frontal electroencephalogram (EEG), primary motor cortical local field
734 potentials (LFP), corresponding raw signal with multi-unit activity (MUA), and detected spikes, in
735 representative segments of waking and NREM sleep. Slow waves and synchronous spiking off periods
736 are visible in NREM sleep but not in wakefulness. **C)** The distribution of mean firing rates during wake,
737 NREM and REM sleep over the whole dataset, in addition to the difference in mean firing rates in wake
738 compared to NREM sleep (all are positive, reflecting higher firing in wake). Points indicate channels
739 grouped by animal (left to right), but boxplots reflect channels from all animals treated as one
740 population. **D)** Distribution of correlation coefficients, calculated within each single channel, between
741 wake episode duration (Duration), the change in slow wave activity (dSWA), and mean firing rate (mean
742 FR). Points indicate channels grouped by animal (left to right), but boxplots reflect channels from all
743 animals treated as one population. **E)** An example scatter plot of the correlation between the change in
744 median SWA from one NREM episode to the next and the mean firing rate during the intervening period
745 of wakefulness. This channel is representative because it has the median correlation coefficient of all
746 channels.

747 **Figure 2.** Slow wave activity dynamics at the LFP level can be modelled using multi-unit spiking
748 information. **A)** An example from one representative animal modelling the SWA averaged over all LFP
749 channels, of both the classical model (blue) and novel firing-rate-based model (orange), calculated from
750 the firing rate also averaged over all LFP channels (brown). **B)** An example of both models applied to
751 the SWA of a single LFP channel, which came from the same animal as used in **A**.

752 **Figure 3.** The fit quality and parameters for both classical and firing-rate-based models of LFP SWA. **A)**
753 Equations for the classic state-based model (blue) and novel firing-rate-based model (orange). **B)** For
754 each animal, the distribution over channels of the median difference between the model and empirical

755 SWA, expressed as a percentage of empirical SWA, for both classic and firing-rate-based models. **C)** The
756 same median percent error, grouped over animals and models, separately showing errors at the level of
757 single LFP, averaged LFP and EEG. **D-G)** The distribution of values used for each parameter in the classic
758 model and **H-L)** in the firing-rate-based model, with boxplots plotted separately for each animal. The
759 black lines indicate the values obtained from modelling the averaged LFP SWA and firing rate over all
760 channels within an animal. Additionally, the red lines in **D-G** give the parameter value obtained from the
761 model of the frontal EEG SWA of that animal. **M)** The distribution of the final optimised value for the
762 firing rate set point parameter ($\boldsymbol{F_\theta}$) of the firing-rate-based model, z-normalised to the distribution of
763 firing rates within wake, NREM and REM sleep. Points indicate channels grouped by animal (left to
764 right), but boxplots reflect all channels treated as one population. **N)** The distribution of mean firing rate
765 in wake, NREM and REM sleep, expressed as a percentage of the firing rate set point parameter ($\boldsymbol{F_\theta}$).
766 Points indicate channels grouped and coloured by animal, but boxplots reflect all channels treated as
767 one population. **O)** The distribution of the change in Process S ($\boldsymbol{\Delta S/\Delta t}$) from one 4-s time step to the next
768 derived from the Fr-SWA model in wake, NREM sleep and REM sleep. All mice, channels and time are
769 pooled. Source data is provided for this figure which contains all simulated Process S time courses,
770 model parameters and the data required to reproduce them.

771 **Figure 4.** The definition of off periods and off occupancy. **A)** An example section of LFP (raw in grey,
772 0.5-6Hz filtered in black) and simultaneous MUA spikes. During this time window, the filtered LFP
773 crosses above the amplitude threshold (265 μV for this channel, red line) five times. The multi-unit inter-
774 spike interval aligned to two of these peaks exceeds the duration threshold (85ms for this channel) and
775 so two off periods are detected (grey boxes). ISIs aligned to the other three out of five crossings
776 (asterisks) are too short to be considered off periods. **B)** Histograms of multi-unit inter-spike intervals
777 aligned with detected slow waves for this example channel. The four plots show, from left to right, ISIs
778 over the whole recording and ISIs separately during wake, NREM and REM sleep only. The ISI duration
779 threshold (red line) is selected using the histogram of all ISIs (leftmost) at the minimum between the
780 two modes. **C)** The distribution of LFP amplitude and **D)** ISI duration threshold values used for definition
781 of off periods for each channel, with boxplots plotted separately for each animal. **E)** The mean multi-unit
782 firing rate over a period of 1 s centred on the peak of detected slow waves, calculated over all slow waves

783 within one example channel with a resolution of 1 ms. **F)** Distributions of mean off occupancy (%) for
784 all channels averaged over wake, NREM and REM sleep. Points indicate channels grouped by animal (left
785 to right), but boxplots reflect all channels treated as one population. **G)** Off occupancy is shown alongside
786 EEG and LFP SWA for an example channel over 48 hours. Traces represent these values calculated at 4-
787 s resolution (light grey), in addition to the median value per NREM sleep episode, as used for model
788 fitting (black bars). Firing rate (brown) and scored vigilance states are also shown.

789 **Figure 5.** Process S is reflected in an LFP channel's off occupancy and its dynamics are described well
790 by both state-based and firing-rate-based models. **A)** An example of the novel model based on firing
791 rates and off occupancy (purple), and the classic state-based model (blue), with optimised parameters
792 describing the dynamics of off occupancy (median per NREM episode, black bars) over 48 hours. Sleep
793 deprivation occurred as indicated at light onset of the second day and lasted 6 hours. Firing rate
794 (brown), off occupancy (value per 4-s epoch, grey) and scored vigilance states are also shown. **B)**
795 Equations for the classic state-based model (blue) and firing-rate-and-off-occupancy-based model for
796 off occupancy (purple). **C)** For each animal, the distribution over channels of the median difference
797 between the model and empirical off occupancy, expressed as a percentage of the off occupancy, for both
798 classic and firing-rate-based models. **D)** The distribution of values of the change in Process S ($\boldsymbol{\Delta S/\Delta t}$)
799 from one 4-s time step to the next derived from the Fr-SWA model in wake, NREM sleep and REM sleep.
800 All mice, channels and time are pooled. **E-H)** The distribution of optimised values used for each
801 parameter in the classic model and **I-L)** the firing rate model, with boxplots plotted separately for each
802 animal. Source data is provided for this figure which contains all simulated Process S time courses,
803 model parameters and the data required to reproduce them.

804 **Figure 6.** The time course of Process S is similar between models and individual channels. Process S
805 time courses, expressed for each channel as a percentage of the maximum value, overlaid for all channels
806 within a single representative animal obtained from **A)** the classic state-based model applied to LFP
807 SWA, **B)** the firing-rate-based model applied to LFP SWA, **C)** the classic state-based model applied to off
808 occupancy, **D)** the firing-rate-based model applied to off occupancy. In these panels the black line
809 indicates the mean Process S over all channels. **E)** The mean Process S calculated over all channels is

now plotted in colour (Cl-SWA light blue, Fr-SWA orange, Cl-Off dark blue, Fr-Off purple), and the red line indicates the Process S obtained by applying model Cl-SWA to the EEG derived SWA.

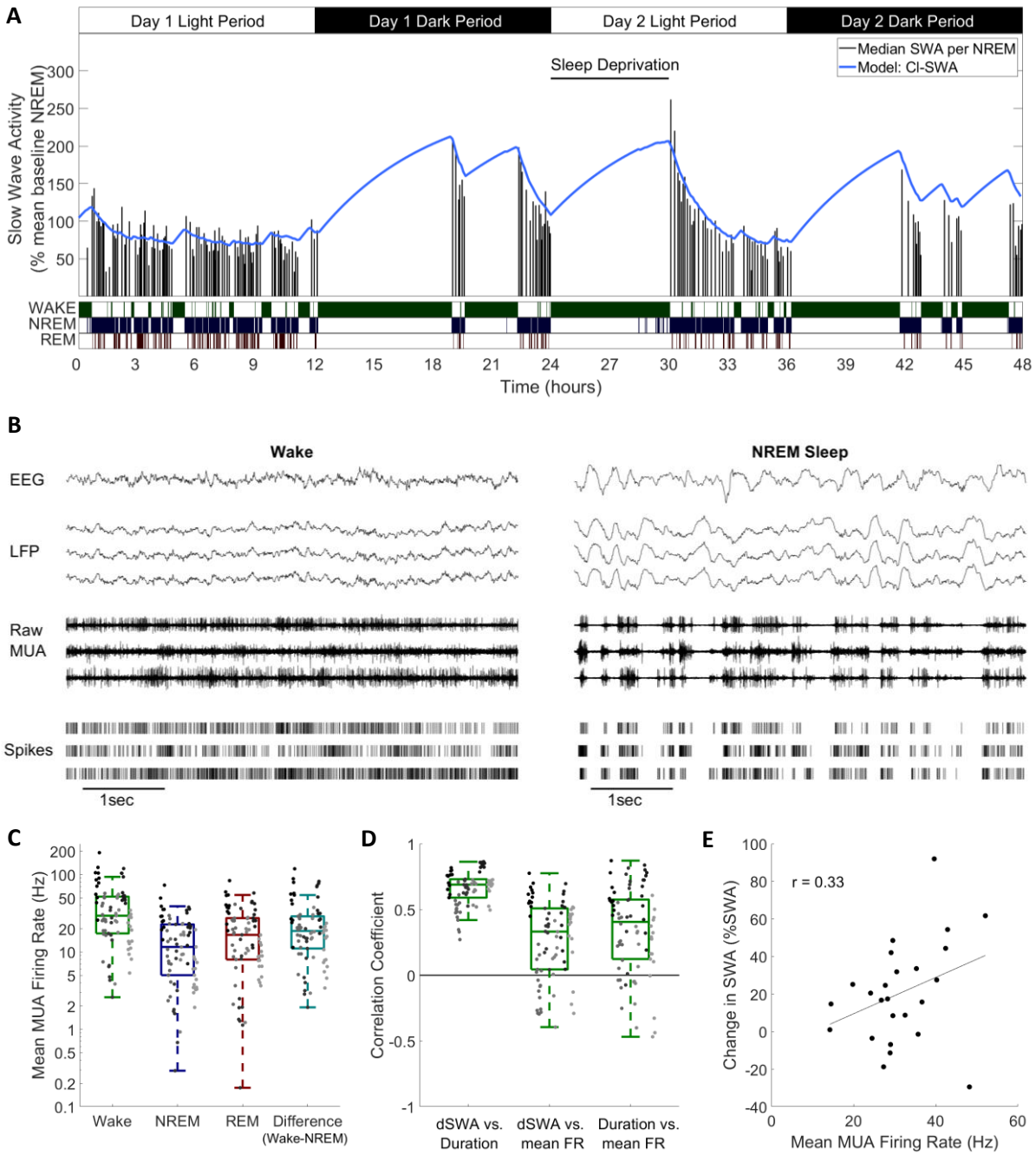
A
Day 1 Light Period
Day 1 Dark Period
Day 2 Light Period
Day 2 Dark Period
Sleep Deprivation
Median SWA per NREM
Model: CI-SWA
Slow Wave Activity (% mean baseline NREM)
WAKE
NREM
REM
Time (hours)
B
Wake
NREM Sleep
EEG
LFP
Raw
MUA
Spikes
1sec
C
Mean MUA Firing Rate (Hz)
Wake
NREM
REM
Difference (Wake-NREM)
D
Correlation Coefficient
dSWA vs. Duration
dSWA vs. mean FR
Duration vs. mean FR
E
r = 0.33
Change in SWA (%SWA)
Mean MUA Firing Rate (Hz)

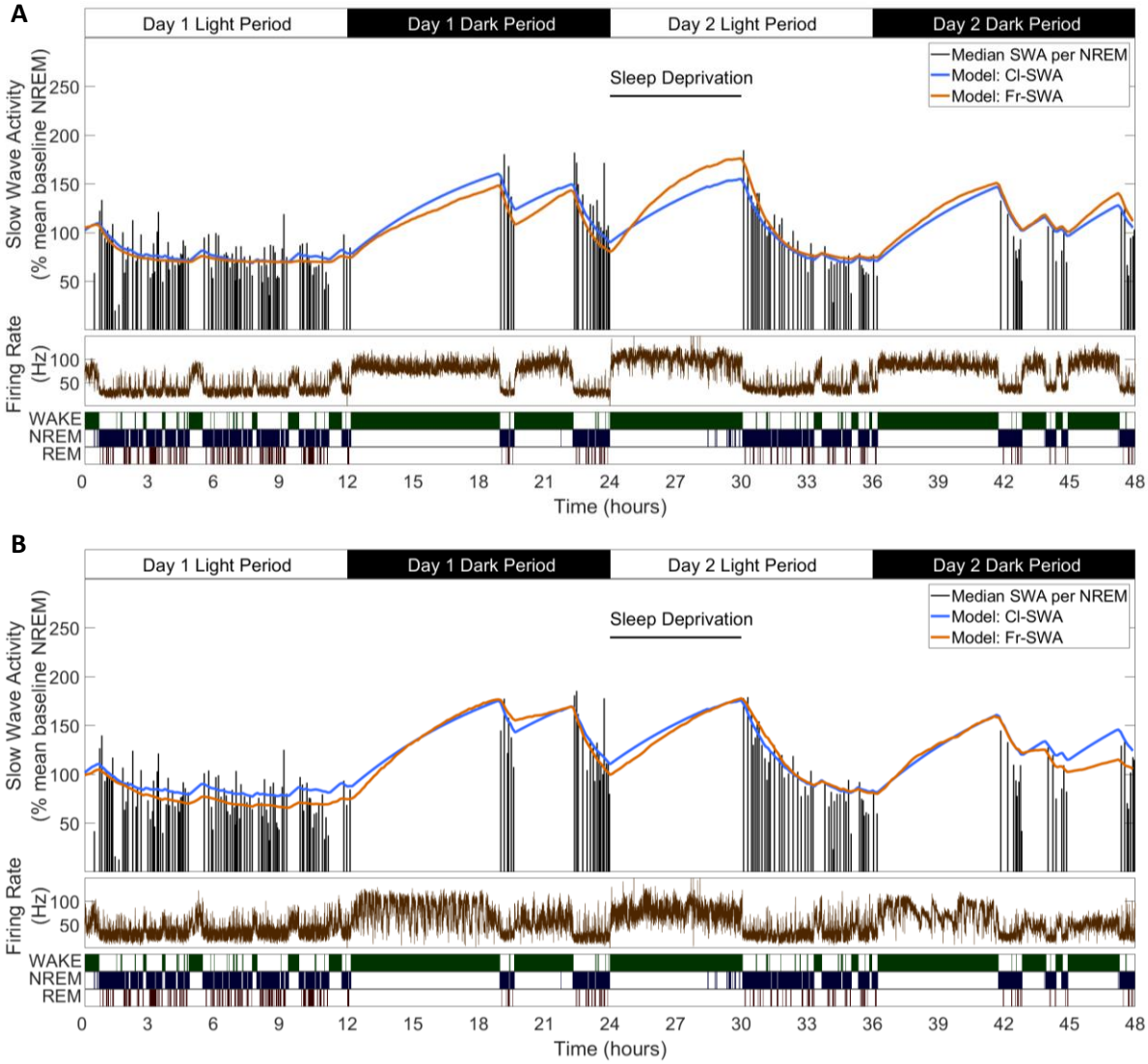
A
Day 1 Light Period
Day 1 Dark Period
Day 2 Light Period
Day 2 Dark Period
Sleep Deprivation
Median SWA per NREM
Model: Cl-SWA
Model: Fr-SWA
Slow Wave Activity
(% mean baseline NREM)
Firing Rate
(Hz)
WAKE
NREM
REM
Time (hours)
B
Day 1 Light Period
Day 1 Dark Period
Day 2 Light Period
Day 2 Dark Period
Sleep Deprivation
Median SWA per NREM
Model: Cl-SWA
Model: Fr-SWA
Slow Wave Activity
(% mean baseline NREM)
Firing Rate
(Hz)
WAKE
NREM
REM
Time (hours)

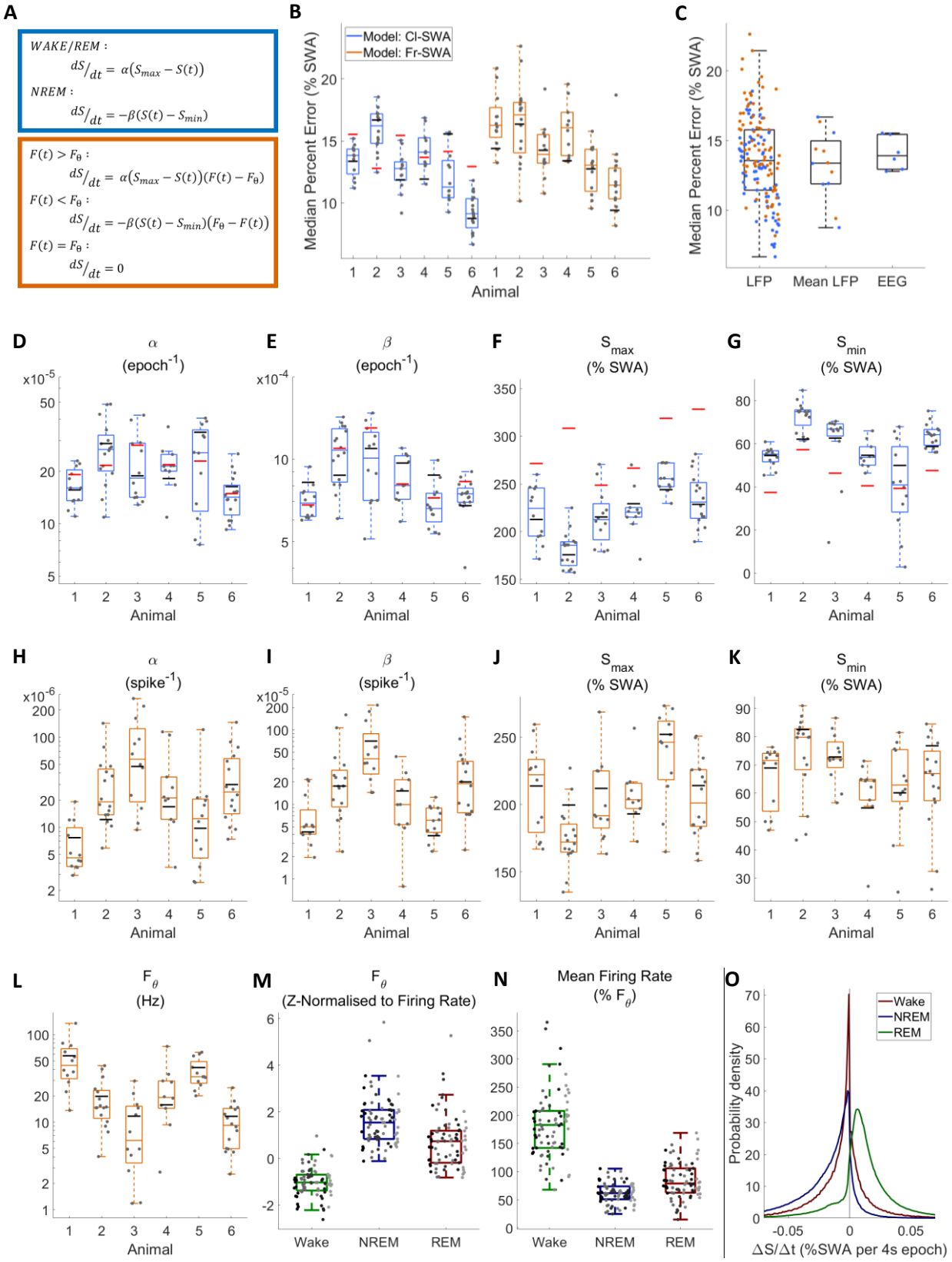
A
WAKE/REM :
$dS/dt = \alpha(S_{max} - S(t))$
NREM :
$dS/dt = -\beta(S(t) - S_{min})$
$F(t) > F_\theta$:
$dS/dt = \alpha(S_{max} - S(t))(F(t) - F_\theta)$
$F(t) < F_\theta$:
$dS/dt = -\beta(S(t) - S_{min})(F_\theta - F(t))$
$F(t) = F_\theta$:
$dS/dt = 0$
B
Model: Cl-SWA
Model: Fr-SWA
Median Percent Error (% SWA)
Animal
C
Median Percent Error (% SWA)
LFP
Mean LFP
EEG
D
α (epoch^{-1})
E
β (epoch^{-1})
F
S_{max} (% SWA)
G
S_{min} (% SWA)
H
α (spike^{-1})
I
β (spike^{-1})
J
S_{max} (% SWA)
K
S_{min} (% SWA)
L
F_θ (Hz)
M
F_θ (Z-Normalised to Firing Rate)
N
Mean Firing Rate (% F_θ)
Wake
NREM
REM
O
Probability density
ΔS/Δt (%SWA per 4s epoch)

Figure 3

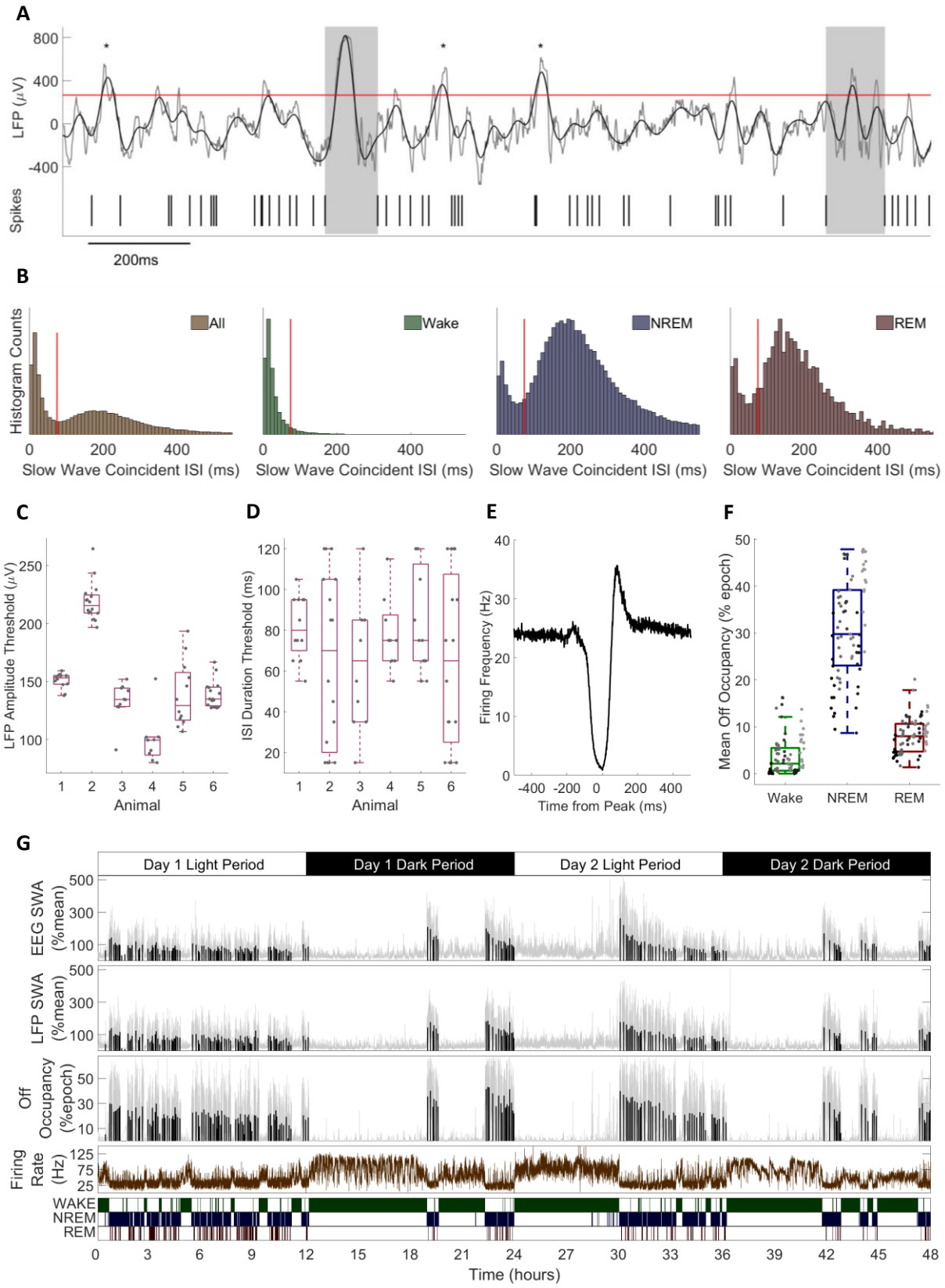
A
LFP (μV)
Spikes
200ms
B
Histogram Counts
All
Wake
NREM
REM
Slow Wave Coincident ISI (ms)
C
LFP Amplitude Threshold (μV)
Animal
D
ISI Duration Threshold (ms)
Animal
E
Firing Frequency (Hz)
Time from Peak (ms)
F
Mean Off Occupancy (% epoch)
Wake
NREM
REM
G
Day 1 Light Period
Day 1 Dark Period
Day 2 Light Period
Day 2 Dark Period
EEG SWA (%mean)
LFP SWA (%mean)
Off Occupancy (%epoch)
Firing Rate (Hz)
WAKE
NREM
REM
Time (hours)

Figure 4

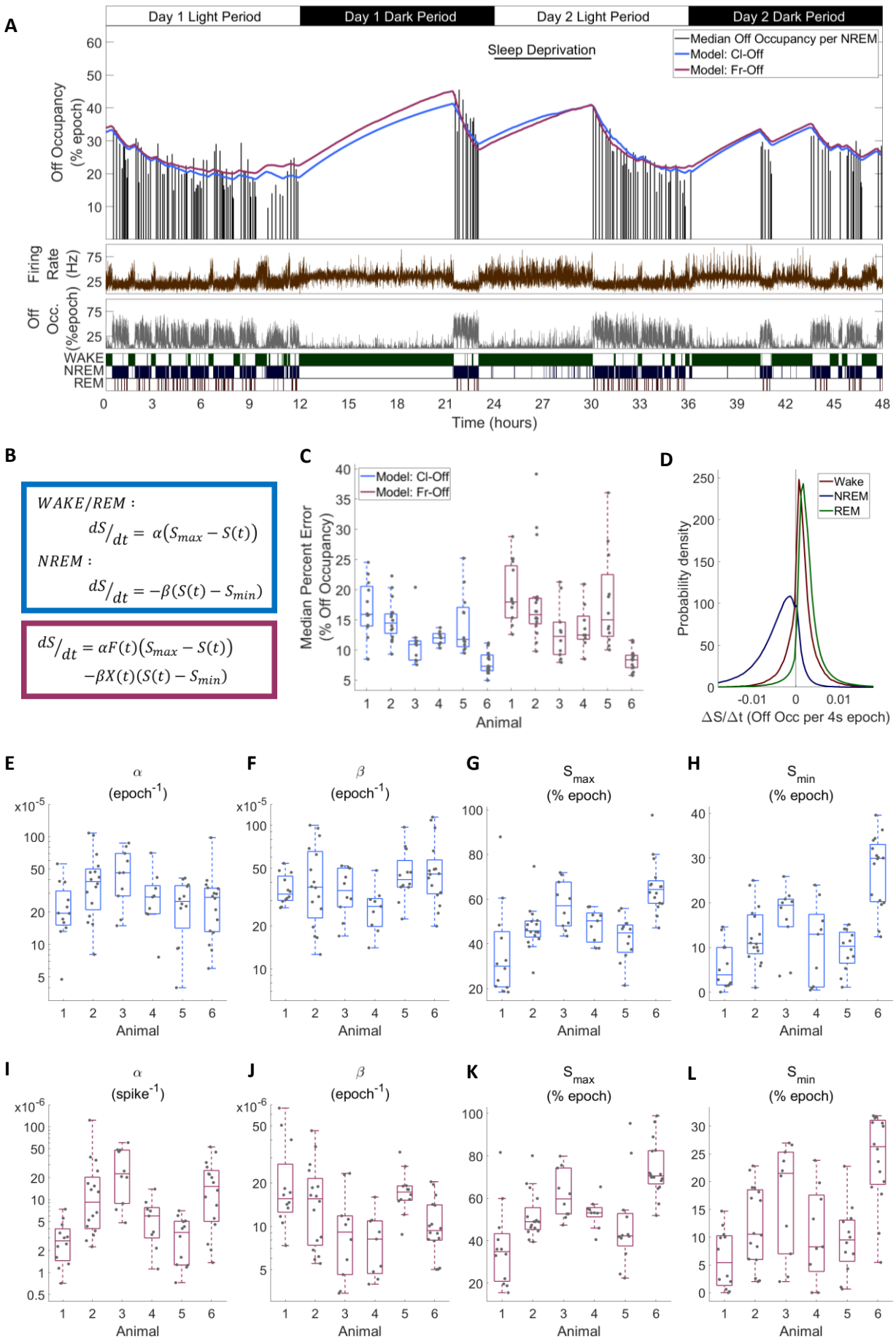
A
Day 1 Light Period
Day 1 Dark Period
Day 2 Light Period
Day 2 Dark Period
Sleep Deprivation
Median Off Occupancy per NREM
Model: Cl-Off
Model: Fr-Off
Off Occupancy (% epoch)
Firing Rate (Hz)
Off Occ. (%epoch)
WAKE
NREM
REM
Time (hours)
B
WAKE/REM :
$dS/dt = \alpha(S_{max} - S(t))$
NREM :
$dS/dt = -\beta(S(t) - S_{min})$
$dS/dt = \alpha F(t)(S_{max} - S(t)) - \beta X(t)(S(t) - S_{min})$
C
Model: Cl-Off
Model: Fr-Off
Median Percent Error (% Off Occupancy)
Animal
D
Wake
NREM
REM
Probability density
ΔS/Δt (Off Occ per 4s epoch)
E
α (epoch^{-1})
F
β (epoch^{-1})
G
S_{max} (% epoch)
H
S_{min} (% epoch)
I
α (spike^{-1})
J
β (epoch^{-1})
K
S_{max} (% epoch)
L
S_{min} (% epoch)
Animal

Figure 5

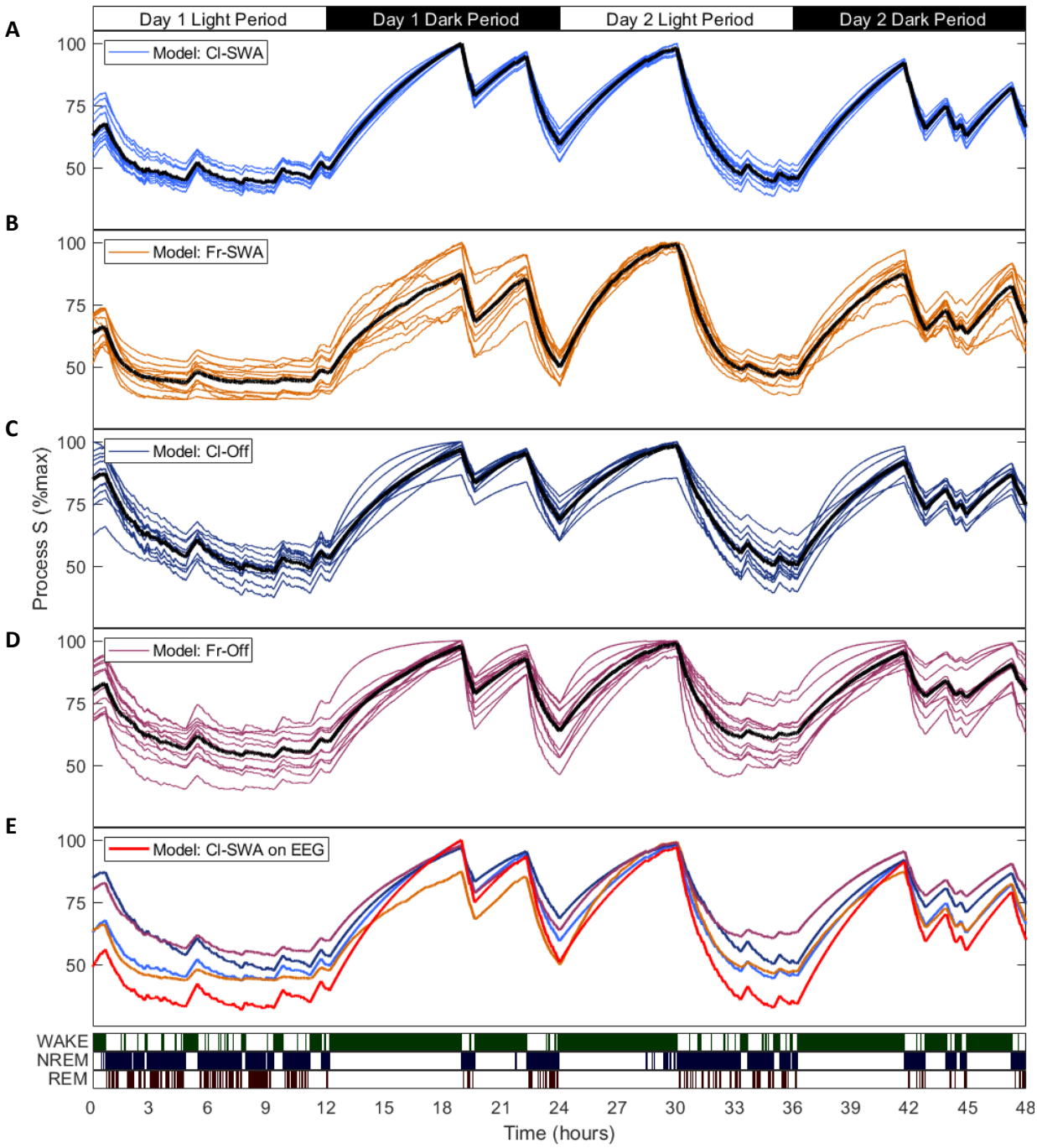
Day 1 Light Period
Day 1 Dark Period
Day 2 Light Period
Day 2 Dark Period
A
Model: Cl-SWA
B
Model: Fr-SWA
C
Model: Cl-Off
D
Model: Fr-Off
E
Model: Cl-SWA on EEG
Process S (%max)
100
75
50
WAKE
NREM
REM
0
3
6
9
12
15
18
21
24
27
30
33
36
39
42
45
48
Time (hours)

Figure 6